

LIFE: Lighting Invariant Flow Estimation

Zhaoyang Huang^{1,3*}
Ka Chun Cheung³

Xiaokun Pan^{2*}
Guofeng Zhang²

Runsen Xu²
Hongsheng Li¹

Yan Xu¹

¹CUHK-SenseTime Joint Laboratory, The Chinese University of Hong Kong

²State Key Lab of CAD&CG, Zhejiang University

³NVIDIA AI Technology Center, NVIDIA

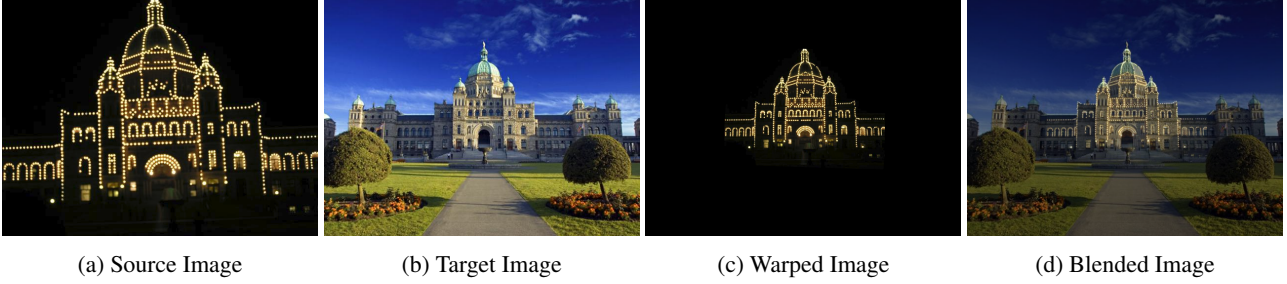


Figure 1: Image warping with flows predicted by LIFE.

Abstract

We tackle the problem of estimating flow between two images with large lighting variations. Recent learning-based flow estimation frameworks have shown remarkable performance on image pairs with small displacement and constant illuminations, but cannot work well on cases with large viewpoint change and lighting variations because of the lack of pixel-wise flow annotations for such cases. We observe that via the Structure-from-Motion (SfM) techniques, one can easily estimate relative camera poses between image pairs with large viewpoint change and lighting variations. We propose a novel weakly supervised framework LIFE to train a neural network for estimating accurate lighting-invariant flows between image pairs. Sparse correspondences are conventionally established via feature matching with descriptors encoding local image contents. However, local image contents are inevitably ambiguous and error-prone during the cross-image feature matching process, which hinders downstream tasks. We propose to guide feature matching with the flows predicted by LIFE, which addresses the ambiguous matching by utilizing abundant context information in the image pairs. We show that LIFE outperforms previous flow learning frameworks by large margins in challenging scenarios, consistently improves feature matching, and benefits downstream tasks.

1. Introduction

Establishing correspondences between image pairs is a fundamental problem in 3D computer vision, which supports many downstream applications, such as relative pose estimation [27, 51], visual localization [40], homography estimation [59, 16], etc. Pixel-wise dense correspondences further enable image editing [19, 23], 3D reconstruction [1], etc. Fully supervised flow estimation methods [47, 10, 48] have achieved satisfactory performance for consecutive frames, which usually have similar lighting conditions and pixel displacements between image pairs are usually limited. In more general scenes, there may exist large viewpoint and illumination changes between pairs of images. However, annotating dense correspondences by humans for flow estimation is infeasible for such scenarios as the number of pixels is quite large. To alleviate the impact of large viewpoint change for flow prediction, there were previous research [38, 49] that synthesizes the second image by applying geometric transformations to an image. Although the accurate dense correspondences with large pixel displacements can be accurately obtained from the geometric transformations in this way, the synthesized images still cannot mimic realistic illumination variations and do not conform to actual geometric transformations.

With the mature Structure-from-Motion (SfM) technology [43], we can collect images of the same scene from the Internet and accurately estimate their camera poses in a unified coordinate system. Due to the large time span of these

*Zhaoyang Huang and Xiaokun Pan assert equal contributions.

images, the lighting and viewpoint of the images can significantly vary, and their actual variations cannot be easily synthesized via simple image transformations. Based on such image pairs with large illumination variations and ground-truth relative pose transformations, we propose the Lighting Invariant Flow Estimation (LIFE) framework that trains a deep neural network to estimate flow with such image-level weak supervisions.

According to epipolar geometry [55], the fundamental matrix deduced from the relative camera pose constrain each pixel in the source image to correspond to a line, referred to as epipolar line, in the target image. If we select a pixel in the target image as the correspondence, the distance from the pixel to the epipolar line is named *epipolar distance* and it is expected to be zero, which has been widely used to constrain the searching space of optimization-based optical flow estimation [52, 54]. Besides, once the corresponding pixel is selected, it also corresponds to an epipolar line in the source image, from which we can compute another epipolar distance. The sum of these two distances is *the symmetric epipolar distance*. DFE [34] introduced it as a loss to learn to estimate the fundamental matrix with given correspondences. Inspired by them, we alternate the learning objective in DFE: via minimizing the symmetric epipolar distance loss, we can train a neural network to estimate dense pixel flows, given an image pair with a given fundamental matrix. Thanks to the adequate training data with different lighting conditions, our LIFE can learn robust feature representations against severe lighting variations.

The proposed symmetric epipolar distance loss only imposes weak constraints on the flow estimation, which allows the predicted flow to slide along the corresponding epipolar line. To improve the accuracy of flow, we synthesize an image from one image in the image pair with geometric transformations. The additional pixel-to-pixel constraint derived from the geometric transformations further complements the symmetric epipolar distance loss and achieves accurate lighting-invariant flow estimation. We present an example that warps an image captured at nighttime to an image captured at daytime via the flows predicted by LIFE (Fig. 1).

Besides dense correspondences, establishing sparse correspondences is also an important vision task, which is usually achieved by extracting salient feature points and matching the points according to descriptors. However, as descriptors of feature points are individually extracted from an image with a limited perception field, descriptors from repeated patterns may be indistinguishable. Feature points with ambiguous descriptors are easily erroneously matched during inference, which raises the outlier ratio and might impact downstream tasks. Guiding feature matching with flows is a common strategy in recent visual odometry [32], which alleviates the descriptor ambiguity and reduces computational complexity. Nonetheless, it is not utilized in

other applications such as visual localization as previous methods have difficulties in flow estimation for images with large lighting variations. We propose to improve the sparse feature matching with the flows predicted our proposed LIFE. To our best knowledge, we are the first to explicitly address the lighting variation problem of direct flow prediction with the epipolar constraints as weak supervisions and also make use of lighting-invariant flows to improve feature matching in practical scenarios. With the assist of our LIFE, the inlier ratio of sparse correspondences increases and the accuracy of the follow-up geometric transformation estimation is significantly improved.

In summary, our proposed approach has the following major contributions: (1) We propose a weakly supervised framework LIFE that trains the flow estimation neural network with camera pose transformations and can predict accurate flow in large viewpoint and lighting variation scenarios. (2) We propose to improve the sparse feature matching with our predicted lighting invariant flows, which is able to alleviate the ambiguity of local descriptor matching. (3) Our proposed LIFE outperforms state-of-the-art flow estimation methods in challenging scenes by large margins and improves sparse feature matching performance to assist downstream applications.

2. Related Works

Learning to estimate flow Great efforts have been devoted to estimate flow between image pairs in the past four decades. With the success of deep neural networks, learning-based flow estimation has achieved impressive results. A common optical flow estimation scene is to find pixel correspondences in two consecutive images of a video. Dosovitskiy *et al.* [5] constructed FlowNet, the first end-to-end trainable CNN for predicting optical flow and trained it on the synthetic FlyingChairs dataset. Since then, a great number of works [12, 35, 46, 47, 10, 11, 61, 48] are proposed for improving the neural network architecture. RAFT [48] achieves the best performance with full supervision in all public optical flow benchmarks by utilizing a multi-scale 4D correlation volume for all pairs of pixels and a recurrent unit iteratively updating the flow estimation. Learning flow estimation requires ground-truth pixel-wise annotations, but it is too expensive in real scenes. Some unsupervised learning [13, 36, 25, 58, 62, 21] frameworks circumvent this requirement by utilizing image warping loss and geometry consistency [58, 62, 21]. However, consecutive images under good lighting conditions is a rather simple case and image warping loss assumes constant illumination. Researchers have recently started to address flow estimation in more challenging scenarios where annotating pixel-wise flow for training becomes even more difficult, such as low-light [60] or foggy [56] images. They address the data problem by image synthesize [60] or domain transforma-

tion [56]. Large viewpoint and illumination transformation will also significantly increase the difficulty of flow estimation. [49, 50, 26, 38] focus on improving the neural network architecture for large viewpoint change. The training data is maintained by applying geometric transformations to images, which is not in line with real scenes. To alleviate the impact from illumination variation, Simon *et al.* [25] use the ternary census transform [45] to compensate for additive and multiplicative illumination change but it is a simple handcrafted approximation. RANSAC-Flow [44] estimates flow with an off-the-shelf feature extractor and the RANSAC [7, 33] based on multiple homographies, which presents good performance but the resultant flows are restricted by the multiple homographies.

Learning with Epipolar Constraints Correspondences anchored upon the surfaces of rigid objects between two views must obey the geometric transformation according to the relative pose, which is called epipolar constraints. As most contents in images are static and rigid, epipolar constraints are widely employed in traditional optimization-based optical flow [52, 54, 55]. Recently, epipolar constraints are introduced to construct loss functions for learning. Subspace constraint and low-rank constraint [61] are applied in unsupervised optical flow learning. Some local feature learning methods leveraged epipolar constraints to train detectors [57] and descriptors [53]. Ranftl *et al.* [34] learned to estimate fundamental matrix from given correspondences with the symmetric epipolar distance loss. Reducing the correspondence searching space to a narrow band along the epipolar line [9] is also a common strategy. To our best knowledge, we are the first that directly learn flow by the symmetric epipolar distance loss. Fueled by abundant and various training data maintained from SfM, LIFE is robust to large viewpoint and illumination change.

3. Method

We propose the weakly supervised lighting invariant flow estimation (LIFE) framework, which only requires whole-image camera pose transformations as weak supervisions and shows effectiveness on establishing accurate and dense correspondences between images with significant lighting and viewpoint variations. In this section, we will elaborate the LIFE framework and the LIFE-based sparse correspondences establishment. The neural network architecture of RAFT [48] has been proven successful in learning optical flows but it only learns to predict flows from a source image to a target image. We use RAFT to predict flows in both source-to-target and target-to-source directions with shared parameters as our training losses are applied in both directions. Training data are prepared as image pairs with corresponding fundamental matrices, which can be easily obtained from the Internet and processed by SfM techniques to recover the camera poses. Because of

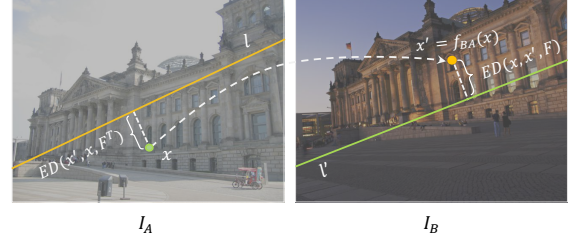


Figure 2: Symmetric epipolar distance.

the weak supervisions from whole-image camera poses, we further regularizing the flow learning with cycle consistency and synthetic dense flows. Finally, we show how to establish highly accurate sparse correspondences with the bidirectional flows predicted by LIFE.

3.1. Training Light-invariant Dense Flows from Camera Poses

As camera poses between images with large appearance and geometric variations are easier to acquire than dense flows, our proposed LIFE learns from such camera poses as weak supervisions to predict lighting invariant dense flows.

Symmetric Epipolar Distance (SED) loss. Based on the epipolar geometry, we propose a symmetric epipolar distance (SED) loss to achieve this goal. We compute the fundamental matrix F from I_A to I_B according to their camera intrinsic parameters and relative camera pose. As shown in Fig. 2, F restricts that a pixel location $x \in \mathbb{R}^2$ in image I_A can only be mapped to one of the points on a line $l' = Fx$, referred to as *epipolar line* in image I_B . For each point x in image I_A , our network estimates its corresponding point in image I_B as $x' = f_{B \leftarrow A}(x)$. If the A -to- B flows are ideal, the distance of the corresponding pixel location x' to the epipolar line l' , named epipolar distance (ED), shall be zero. Reversely, x is also supposed to lie on the epipolar line l derived from x' in image I_B if the reverse flows are ideal, and the distance from x to the epipolar line l should also be zero. The sum of the two epipolar distances is defined as the symmetric epipolar distance (SED). According to the epipolar geometry, the inverted fundamental matrix equals the transpose of the fundamental matrix, we can therefore compute the SED as

$$SED(x, x', F) = ED(x, x', F) + ED(x', x, F^T). \quad (1)$$

Given the A -to- B dense flows $f_{B \leftarrow A}$ predicted by our flow network, we can define the following SED loss to evaluate their accuracies by computing SED for all flows in $f_{B \leftarrow A}$.

$$L_{SED} = \sum_{x_i \in S} SED(x_i, f_{B \leftarrow A}(x_i), F), \quad (2)$$

where S is the set containing all pixel locations in I_A . Compared with photometric consistency loss used in existing unsupervised flow learning frameworks, which assumes constant lighting conditions, the proposed epipolar distance loss is only determined by the fundamental matrix (or relative camera pose). Therefore, the SED loss works even when there exist significant lighting variations between the two images.

Cycle consistency regularization. The cycle loss measuring flows' cycle consistency $d(\mathbf{x}) = \|f_{A \leftarrow B}(f_{B \leftarrow A}(\mathbf{x})) - \mathbf{x}\|_2$ is a common regularization term in correspondence learning [39]. However, pixels in occluded regions do not satisfy the cycle consistency assumption and might infer large cycle distance errors to overwhelm the cycle loss. Therefore, making all flows to be cycle consistent would actually hinder the training and generate over-smooth flow fields with degraded performances. Inspired by unsupervised optical flow learning [25, 58], we filter out pixels with too large cycle distance errors and use the cycle loss from the kept pixels.

$$L_{cyc} = \sum_{\mathbf{x}_i \in S} \mathbf{1}(d(\mathbf{x}_i) \leq \max\{\alpha, \beta \|f_{B \leftarrow A}(\mathbf{x}_i)\|_2\}) d(\mathbf{x}_i),$$

where $\mathbf{1}$ denotes the indicator function. A pixel \mathbf{x} whose cycle distance is larger than α and $\beta \|f_{B \leftarrow A}(\mathbf{x})\|_2$ will be filtered in the cycle loss.

Synthetic dense-flow regularization. Although the SED loss can work on image pairs of actual scenes with significant lighting and pose variations, it can only provide weak supervision on minimizing the distances from points to their epipolar lines. In other words, as long as the predicted flow aligns points to their epipolar lines in the other image, their SED loss is minimal. However, points' ground-truth correspondences should also be single points. In order to improve the accuracy of the flow prediction, we propose to regularize the estimated flows with synthetic pixel-to-pixel supervisions. Inspired by Rocco *et al.* [38], for each image pair, we randomly generate an affine or thin-plate spline transformation \mathbf{T} to transform image I_B of the image pair. In this way, we can create a synthesized image $I_{B'}$ and a synthesized image pair $\langle I_B, I_{B'} \rangle$ (Fig. 3) with accurate dense pixel-to-pixel correspondence ground truth. Given the location of a pixel in I_B , we can compute its accurate corresponding location in $I_{B'}$ according to the synthesized geometric transformation \mathbf{T} , and vice versa via the inverse of the geometric transformation \mathbf{T}^{-1} . We therefore additionally regularize our flow network with a bidirectional geometric transformation (BiT) loss. The BiT loss supervises the bidirectional flow with accurate pixel-to-pixel dense correspondences, but the image pair has a

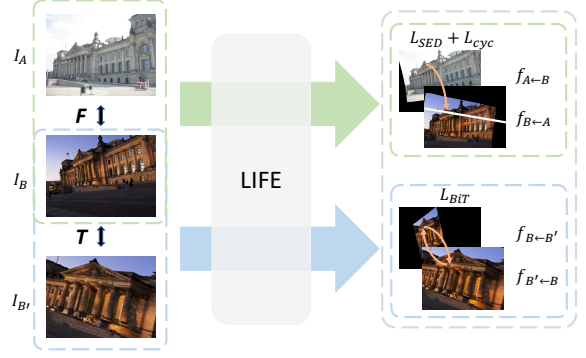


Figure 3: The overall training loss. The top pair with large lighting and viewpoint variation is supervised by the proposed Symmetric Epipolar Distance (SED) loss and the cycle consistency loss. The bottom pair with a synthetic transformation is supervised by the bidirectional geometric transformation (BiT) loss.

synthetic image transformation and zero lighting variation,

$$L_{BiT} = \sum_{\mathbf{x}_i \in S_B} \|f_{B' \leftarrow B}(\mathbf{x}_i) - \mathbf{T}(\mathbf{x}_i)\|_1 + \sum_{\mathbf{x}_i \in S_{B'}} \|f_{B \leftarrow B'}(\mathbf{x}_i) - \mathbf{T}^{-1}(\mathbf{x}_i)\|_1, \quad (3)$$

where S_B and $S_{B'}$ contains locations of valid pixels in I_B and $I_{B'}$ respectively. For points that might be out of the visible region in the target images, we regard these flow as invalid and filter out them for loss computation.

The overall loss. For image I_B and its synthetically transformed version $I_{B'}$, I_B is related to I_A according to their fundamental matrix \mathbf{F} , while the dense correspondences between I_B and $I_{B'}$ are precisely determined by the synthesized geometric transformation \mathbf{T} . We apply the SED loss and the cycle loss to the bidirectional flow deduced from I_A and I_B , and the BiT loss to the bidirectional flow deduced from I_B and $I_{B'}$ (Fig. 3). The SED loss supervises flows between actual image pairs with natural lighting and viewpoint variations but only provides weak supervision signals. On the contrary, the BiT loss regularizes flow with strict dense correspondences with constant lighting conditions and synthesized image transformation. Unifying the losses of the images can simultaneously mitigate both their drawbacks and contribute to training a robust lighting-invariant flow estimation network.

3.2. Finding Sparse Correspondences with LIFE

Dense correspondences can be used in many applications but are not mandatory in whole-image geometric transformation estimation tasks, such as relative pose estimation and homography estimation. In such tasks, we only

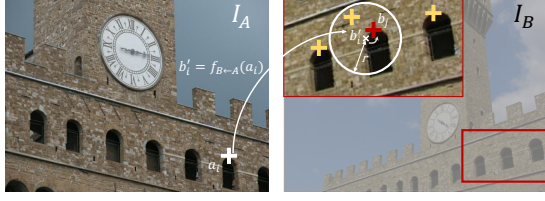


Figure 4: With the flow predicted by LIFE, we find the feature point \mathbf{b}_j whose descriptor is the closest to that of \mathbf{a}_i in the circle as the corresponding point.

need a small number of sparse but accurate correspondences to estimate whole-image transformation. Sparse correspondences can be generally obtained by detecting locally salient feature points in the image pair with feature descriptors and establishing correspondences between feature points with similar descriptors. However, descriptors encode contents of local image patches, which are inevitably ambiguous in terms of the global image context. Erroneous matches caused by ambiguous descriptors is a long-standing problem even with learning-based descriptors, which both reduce inlier ratio and the number of effective correspondences for the follow-up transformation estimation step. In contrast, our dense flows are less possible to be trapped by local ambiguous patterns thanks to the context information. We design a simple but effective two-stage algorithm to identify sparse correspondences. In stage 1, we identify correspondences with the assist of LIFE. We believe the flows predicted by LIFE are confident, so we only need to find the corresponding features in local regions guided by the predicted flows. The correspondences identified in stage 1 are of high quality but the correspondence number may be unsatisfactorily low because of the strict flow constraints. Therefore, in stage 2, we try to identify more correspondences via the remaining feature points of stage 1.

Stage 1. We denote the sets of sparse feature points detected in I_A and I_B by $\mathbf{a}_i \in A$ and $\mathbf{b}_j \in B$, and denote their descriptors by \mathbf{q}_i^a and \mathbf{q}_j^b . For a given query feature point \mathbf{a}_i , we first calculate its warped point $\mathbf{b}'_i = f_{B \leftarrow A}(\mathbf{a}_i)$ in I_B according to the predicted flows $f_{B \leftarrow A}$. Inside the circle centered at \mathbf{b}'_i , we regard the feature point \mathbf{b}_j whose descriptor is the closest to that of \mathbf{a}_i as the corresponding point (Fig. 4), *i.e.*,

$$\begin{aligned} j &= \arg \max_j \mathbf{q}_i^{aT} \mathbf{q}_j^b, \\ \text{s.t. } \|\mathbf{b}_j - \mathbf{b}'_i\|_2 &\leq r. \end{aligned} \quad (4)$$

r is the radius of the circle, which is set as 5 pixel. In this way, we can try to identify a corresponding feature point \mathbf{b}_j in I_B for each \mathbf{a}_i in I_A , and create a matching feature point set $M_{B \leftarrow A}$ that satisfy the above formula. Reversely, we can use the same strategy to establish a matching point set

$M_{A \leftarrow B}$ in the reverse direction from I_B to I_A . Given the two matching point sets of the two matching directions, we only keep the final matching point pairs as those survive the cycle consistency check, *i.e.*, $\mathbf{x}_i = M_{A \leftarrow B}(M_{B \leftarrow A}(\mathbf{x}_i))$

Stage 2. We collect the features that are weeded out in stage 1 and denote them by A_w and B_w according to which image they belong to. More correspondences are tried to be established from them as supplements. Given a feature point $\mathbf{a}_i \in A_w$ as a query feature, we directly find the feature point $\mathbf{b}_j \in B$ who has the closest descriptor in I_B as its corresponding point. Note that this not equivalent to establishing correspondences between all points A and B with feature descriptors, as A_w and B_w are smaller feature point sets after the stage-1 matching. Similar to stage 1, only the matched point pairs that satisfy the cycle consistency check would eventually be kept. The survived matches are the outcome correspondences in stage 2.

Directly matching local features with descriptors would cause erroneous matches due to the ambiguity of descriptors, which can be corrected by the local match in stage 1 with the guidance of the flows, so the quality of the correspondences highly relies on the flows. Unreliable flows can produce misleading guidance, which may even impact the matching. As LIFE is able to predict accurate flows in challenging scenarios, we can identify more inlier correspondences through this algorithm.

4. Experiments

The core contributions of LIFE are making flow estimation between images with challenging lighting and viewpoint variations practical and addressing the ambiguity problem of sparse feature matching with flows. To demonstrate the effectiveness of LIFE, we compare LIFE with state-of-the-art methods in flow estimation, sparse correspondence establishment, and downstream geometric model estimation. We select R2D2 [37] as the representative local feature for the LIFE-based sparse correspondence identification (LIFE+R2D2). At the end, we perform an ablation study to investigate individual modules and the improvement of LIFE for other local features. More interesting experiments and ablation studies are provided in the supplementary materials and are *strongly recommended*.

Datasets. The MegaDepth dataset [17] collects images under various viewpoint and lighting conditions of 196 scenes and computes their poses with the SfM technique. We solely train LIFE on MegaDepth with camera poses. The scenes used for evaluation have been excluded from training. The HPatches dataset [3] collects image sequences of different scenes under real condition variation. The image sequences can be divided into two subsets: *Viewpoint* captures images with increasing viewpoint change but under the same illumination condition; *Illumination* captures images under increasing illumination but with almost the same

	Viewpoint					Illumination (trans)				
	I	II	III	IV	V	I	II	III	IV	V
CAPS [53]	34.7/72.4	65.2/56.9	76.7/53.8	84.7/48.5	107.6/38.5	26.8/66.7	55.6/52.8	66.0/48.2	78.1/43.6	104.5/35.7
RAFT [48]	15.2/78.0	60.5/49.0	61.8/47.0	67.8/34.8	95.8/25.3	32.6/58.7	93.6/26.9	103.7/25.7	100.6/22.0	141.4/17.3
DGC [26]	5.5/78.4	13.4/66.1	23.3/61.9	38.9/51.0	21.8/41.6	11.5/58.3	23.0/41.6	30.3/32.3	28.9/29.0	45.7/23.9
GLU [49]	0.9/98.6	8.1/91.0	17.1/84.5	19.5/81.0	32.6/67.6	4.8/92.5	15.2/79.7	23.3/76.8	18.0/74.1	37.8/59.4
LIFE	0.9/98.8	6.0/94.6	5.3/94.2	5.3/91.6	11.9/88.0	1.3/95.5	5.8/87.9	13.8/82.9	10.4/85.9	14.6/76.5

Table 1: Flow on HPatches. We compare the AEPE/Acc (%). The difficulty gradually increases from I to V.

	KITTI-2012		KITTI-2015	
	AEPE	F1	AEPE	F1
DGC [26]	8.50	32.28	14.97	50.98
GLU [49]	3.34	18.93	9.79	37.52
GLU+ [50]	3.14	19.76	7.49	33.83
GLU-GOC+ [50]	2.68	15.43	6.68	27.57
UFlow [14]	-	-	9.40	-
DDFlow [20]	8.27	-	17.26	-
R-Flow [44]	-	-	12.48	-
LIFE	2.59	12.94	8.30	26.05

Table 2: Generalization of optical flow on KITTI. + denotes that they use the *dynamic* training strategy.

viewpoint. Each image sequence contains a reference image and 5 source images with increasing variation level. The ground truth homography is provided for all images, so we qualitatively evaluate all the dense correspondences, sparse correspondences, and homography estimation with controlled conditions.

4.1. Flow Evaluation

We evaluate our flows on the KITTI 2012 flow (training), KITTI 2015 flow (training) [8], HPatches [3], RobotCar [24, 15] and MegaDepth datasets [17]. KITTI datasets annotate dense flows between consecutive images, which only have small motion and constant illumination. The KITTI 2015 flow contains more dynamic objects than the KITTI 2012 flow. HPatches contains image pairs with viewpoint and illumination variations of different levels. The dense correspondences used in evaluation is computed from the provided homography. However, these two datasets have certain limitations. To compare the flow prediction performance in real scenes, we further evaluate LIFE on RobotCar [24, 15] and MegaDepth datasets [17]. Dense correspondence annotations are not available in such challenging scenes with large lighting and viewpoint variations. We therefore evaluate the flow performance on provided sparse correspondences.

Dense Flow Estimation on KITTI. We first test flow estimation on the lighting-constant KITTI. We compare LIFE with state-of-the-art unsupervised flow learning methods that are not fine-tuned on KITTI. Following the standard optical flow evaluation protocol, we use the Average End-Point Error (AEPE) and F1 scores in Tab. 2. LIFE achieves

the best performance on the KITTI 2012 flow. Compared with the KITTI 2012 flow, the KITTI 2015 flow contains more dynamic objects. Truong *et al.* [50] introduced a *dynamic* training strategy by augmenting images with random independently moving objects from the COCO [18] so they achieve lower AEPE than our LIFE on the KITTI 2015 flow. Nonetheless, LIFE still has smaller F1 error even without the dynamic training strategy. Moreover, the experiments on KITTI can only demonstrate the flow estimation performance on cases of simple lighting-constant consecutive images, while LIFE focuses on addressing flow estimation in challenging lighting- and viewpoint-varying scenarios, which will be demonstrated in the following experiments.

Dense Flow Estimation on HPatches. We compute the AEPE and accuracy of compared methods in Tab. 1 with increasing levels of difficulty (from I to V). As the image pairs in the *Illumination* subset share the same viewpoint, the ground truth flow is **0** for all pixels, which is too simple. We augment the target images in the *Illumination* subset with generated homographies, so the ground truth flows are no longer all-zero flows. Here, the accuracy is calculated as the percentage of pixels whose endpoint errors are smaller than 5. CAPS [53] learns dense descriptors for feature matching, which establishes dense correspondences by finding the nearest descriptors. It has low accuracy because it does not utilize context information. RAFT [48] is the state-of-the-art supervisory flow estimation method, which fails as well when encountering difficult cases (II-V). DGC-Net [26] and GLU-Net [49] are trained by synthesized images. LIFE consistently outperforms all previous methods and presents increasing superiority from I to V. In Viewpoint (V) and Illumination (V), which include the most challenging cases, LIFE reduces 63.5% and 61.4% AEPE, and raises 20.4% and 17.1% accuracy. These experiments show the remarkable performance of LIFE in the difficult cases with illumination and viewpoint variations.

Sparse Flow Estimation on RobotCar and MegaDepth. These two datasets contain image pairs that correspond to various conditions such as dawn and night. The accuracy of estimating sparse flows are reported in Tab. 3. Following RANSAC-Flow [44], a correspondence is deemed correct if its endpoint error is less than $\epsilon = 1, 3, 5$ pixels. RANSAC-Flow (R-Flow) regularizes flows by RANSAC-based multiple homographies. The images in the MegaDepth are cap-

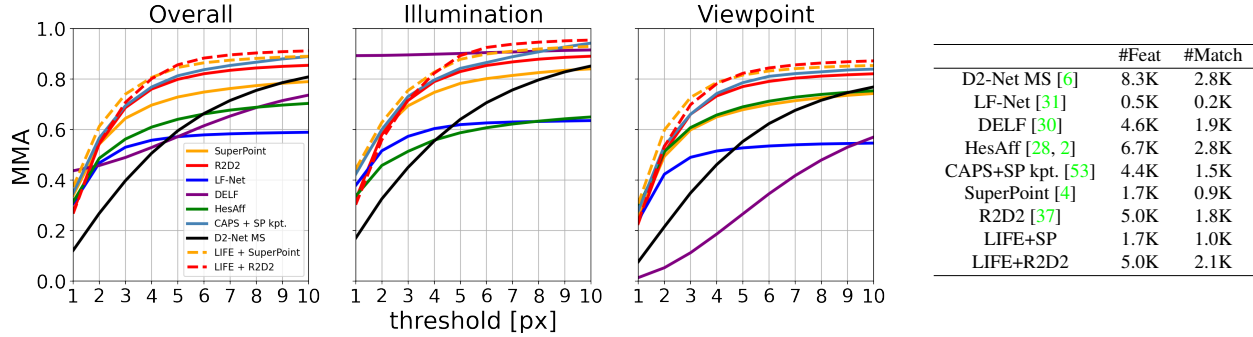


Figure 5: Sparse correspondence identification on HPatches.

ϵ	RobotCar			MegaDepth		
	1	3	5	1	3	5
S-Flow [19]	1.12	8.13	16.45	8.70	12.19	13.30
DGC [26]	1.19	9.35	20.17	3.55	20.33	34.28
GLU [49]	2.16	16.77	33.38	25.2	51.0	56.8
GLU-GOC ⁺ [50]	-	-	-	37.3	61.2	68.1
R-Flow* [44]	2.10	16.07	31.66	53.47	83.45	86.81
LIFE	2.30	17.40	34.30	39.98	76.14	83.14

Table 3: Sparse flow evaluation on RobotCar and MegaDepth. * denotes that RANSAC-Flow explicitly regularizes flows with RANSAC-based multiple homographies.

	MegaDepth			HP
	easy	moderate	hard	$\epsilon = 5$
SIFT [22]	63.9/25.6	36.5/17.0	20.8/13.2	79.0
SuperPoint [4]	67.2/27.1	38.7/18.8	24.5/14.1	90.5
HardNet [29]	66.3/26.7	39.3/18.8	22.5/12.3	-
D2-Net [6]	61.8/23.6	35.2/19.2	19.1/12.2	-
CAPS+SP kpt. [53]	72.9/30.5	53.5/27.9	38.1/19.2	90.7
R2D2 [37]	69.4/30.3	48.3/23.9	32.6/17.4	75.7
LIFE+R2D2	78.7/33.1	62.7/28.7	45.8/22.4	91.2

Table 4: Relative pose estimation on MegaDepth and homography estimation on HPatches.

tured at a long distance, such as bird’s view images, which can fit the homography model well, so it presents remarkable performance on MegaDepth. However, this model does not work in general scenes such as the RobotCar, which takes images with car-mounted cameras. Moreover, we can also use the RANSAC-based multiple homographies as a post-processing strategy to refine flows predicted by other methods if the scenes actually conform to the model. Compared with other methods that directly predict flows without the homography-based refinement, LIFE outperforms all of them on both RobotCar and MegaDepth.

4.2. Sparse Correspondence Identification.

We evaluate LIFE’s effectiveness on sparse correspondence identification based on the HPatches dataset. Following the protocol in D2-Net [6], we use the mean matching accuracy (MMA) and the number of matches as evaluation metrics. As shown in Fig. 5, LIFE can significantly

increase both of the MMA and match number of local features (LIFE+R2D2 v.s. R2D2 and LIFE+SP v.s. SuperPoint). LIFE+R2D2 is slightly inferior at smaller thresholds compared to other methods because the detector of R2D2 is not accurate enough. In contrast, LIFE+SP shows remarkable performance at all thresholds.

4.3. Whole-image Transformation Estimation

In all downstream whole-image transformation estimation tasks, we can see the significant improvement of LIFE+R2D2 based on R2D2, which demonstrates both of the remarkable flow prediction performance of LIFE and the practicability of LIFE-based sparse correspondence identification. We evaluate the LIFE+R2D2 on homography estimation, relative pose estimation, and visual localization.

Homography estimation on HPatches. We use the corner correctness metric introduced by SuperPoint [4], which transforms the four corners of an image respectively using the estimated homography and the ground truth homography, and compute the average pixel error of the transformed four corners. An estimated homography is deemed correct if the average pixel error is less than $\epsilon = 5$ pixels. LIFE increases the accuracy of R2D2 by 15.5% and achieves state-of-the-art performance (Tab. 4).

Relative pose estimation on MegaDepth. We divide the MegaDepth test set into three difficulty levels according to the ground truth relative rotation angle: easy ($[0^\circ, 15^\circ]$), moderate ($[15^\circ, 30^\circ]$) and hard ($[30^\circ, 60^\circ]$). We report the rotation/translation accuracy in Tab. 4. The relative pose is deemed correct if the angle deviation of its rotation or translation is less than 10° . LIFE+R2D2 significantly improves R2D2 and outperforms other methods by large margins.

Visual localization in Aachen. We evaluate the visual localization on the challenging Aachen DayNight benchmark [42]. The reference images used to build the SfM map are all taken during daytime while the query images are capture at nighttime. We report the percentage of query images localized within three given translation and rotation thresholds at nighttime (Tab. 5). LIFE+R2D2 improves the localization accuracy at all thresholds and ranks 1st on the

	0.25m,2°	0.5m,5°	5m,10°
SuperPoint [40]	75.5	86.7	92.9
D2-Net [6]	84.7	90.8	96.9
SuperGlue [41]	86.7	93.9	100.0
R2D2 [37]	80.6	90.8	96.9
LIFE+R2D2	81.6	94.9	100.0

Table 5: Visual localization on Aachen (night).

benchmark at the threshold of (0.5m, 5°) and (5m, 10°).

4.4. Ablation study

Training loss ablation. We investigate individual components of our LIFE on KITTI and HPatches with the AEPE metric. K-12 and K-15 denotes KITTI flow 2012 and KITTI flow 2015. HP-V and HP-I (T) denotes the *Viewpoint* subset and the *Illumination (trans)* subset in HPatches. We assess the effectiveness of our methods by sequentially adding the proposed training losses. T(B'B) denotes that only supervising the network with the flows in one direction of $B' \leftarrow B$ from the synthetic geometric transformation \mathbf{T} . We can see a significant error reduction from T(B'B) to the BiT loss, which indicates the significance of supervising flow prediction in both directions. The KITTI contains consecutive images that share similar lighting conditions. Compared with the SED loss, training with the BiT loss produces less errors on the KITTI because it can provide pixel-to-pixel ground truth. However, it presents worse performance on the HPatches because the synthesized image does not change the illumination and is not in line with the actual situations. In contrast, the SED loss works with image pairs captured in real scenes so it achieves less error on the HPatches. We also test imposing cycle consistency on all flows (denoted by "FC") and adaptive cycle consistency only on small-error pairs (denoted by "AC"). FC impacts the flow estimation because occluded regions in the image do not satisfy cycle consistency, and AC can improve SED on viewpoint change cases. The final model (SED+BiT+AC) that unifies BiT, SED, and AC in the created image triplets achieves the best performance, which demonstrates the SED loss and the BiT loss mitigates their drawbacks well.

LIFE with different local features. We test LIFE with different local features (denoted by "LIFE+*"), including SIFT, SuperPoint, and R2D2 on HPatches. As LIFE-based sparse correspondences are computed in two stages, we also report the performance of outcome matches in stage 1 (denoted by "LIFE+* local"), which are calculated with the guidance of flows predicted by LIFE. We report the MMA, feature number, and match number of corresponding methods in Fig. 6. LIFE consistently improves the MMA and increases the match number. *LIFE+SIFT local*, *LIFE+SP local*, and *LIFE+R2D2 local* all achieves remarkable MMA scores and remains similar match number, which demon-

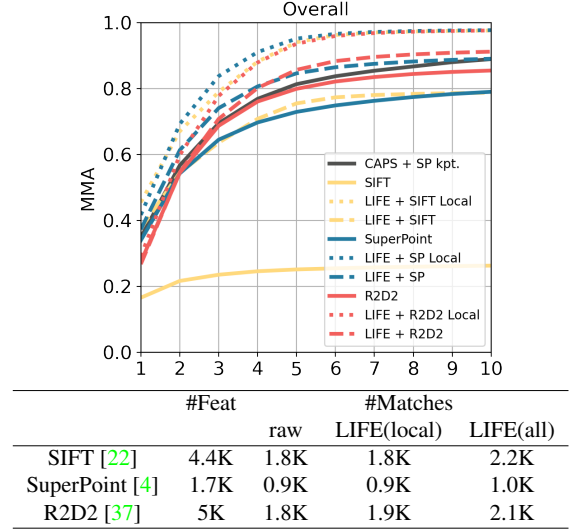


Figure 6: LIFE with different local features.

Training loss	K-12	K-15	HP-V	HP-I(T)
T(B'B)	9.03	27.94	61.03	48.15
BiT	3.71	11.83	16.03	37.6
SED	5.62	16.26	11.69	15.17
SED+FC	6.48	16.83	17.79	23.64
SED+AC	4.89	14.99	12.57	15.47
SED+BiT+AC (Tri)	2.59	8.30	5.90	9.19

Table 6: Ablation study of training losses.

strates the superior performance of LIFE. After introducing the matches established in stage 2 ("LIFE+* local" to "LIFE+*"), the match number increases while the MMA scores decreases because the matches calculated in stage 1 are better than these supplemented matches.

5. Conclusion

We have proposed the weakly supervised framework LIFE that learns flow estimation via whole image camera pose transformations, which can predict dense flows between two images with large lighting variations. With the assist of LIFE, we improved the matching of sparse local features, which increased both of the inlier ratio and match number. The derived sparse correspondences also benefited downstream tasks. In this paper, the dense flow prediction and sparse feature matching are loosely coupled for sparse correspondences establishment, which does not maximize the efficiency of information utilization though can directly adopt off-the-shelf sparse features. Integrating both dense and sparse correspondences estimation into a unified neural network will be the future work. Moreover, LIFE can predict remarkable flows in challenging scenarios, which may enable more downstream applications.

References

- [1] Sameer Agarwal, Yasutaka Furukawa, Noah Snavely, Ian Simon, Brian Curless, Steven M Seitz, and Richard Szeliski. Building rome in a day. *Communications of the ACM*, 54(10):105–112, 2011.
- [2] Relja Arandjelović and Andrew Zisserman. Three things everyone should know to improve object retrieval. In *2012 IEEE Conference on Computer Vision and Pattern Recognition*, pages 2911–2918. IEEE, 2012.
- [3] Vassileios Balntas, Karel Lenc, Andrea Vedaldi, and Krystian Mikolajczyk. Hpatches: A benchmark and evaluation of handcrafted and learned local descriptors. In *Proceedings of the IEEE conference on computer vision and pattern recognition*, pages 5173–5182, 2017.
- [4] Daniel DeTone, Tomasz Malisiewicz, and Andrew Rabinovich. Superpoint: Self-supervised interest point detection and description. In *Proceedings of the IEEE conference on computer vision and pattern recognition workshops*, pages 224–236, 2018.
- [5] Alexey Dosovitskiy, Philipp Fischer, Eddy Ilg, Philip Hausser, Caner Hazirbas, Vladimir Golkov, Patrick Van Der Smagt, Daniel Cremers, and Thomas Brox. FlowNet: Learning optical flow with convolutional networks. In *Proceedings of the IEEE international conference on computer vision*, pages 2758–2766, 2015.
- [6] Mihai Dusmanu, Ignacio Rocco, Tomas Pajdla, Marc Pollefeys, Josef Sivic, Akihiko Torii, and Torsten Sattler. D2-Net: A Trainable CNN for Joint Detection and Description of Local Features. In *Proceedings of the 2019 IEEE/CVF Conference on Computer Vision and Pattern Recognition*, 2019.
- [7] Martin A Fischler and Robert C Bolles. Random sample consensus: a paradigm for model fitting with applications to image analysis and automated cartography. *Communications of the ACM*, 24(6):381–395, 1981.
- [8] Andreas Geiger, Philip Lenz, Christoph Stiller, and Raquel Urtasun. Vision meets robotics: The kitti dataset. *The International Journal of Robotics Research*, 32(11):1231–1237, 2013.
- [9] Yihui He, Rui Yan, Katerina Fragkiadaki, and Shoubo Yu. Epipolar transformers. In *Proceedings of the IEEE/CVF Conference on Computer Vision and Pattern Recognition*, pages 7779–7788, 2020.
- [10] Tak-Wai Hui, Xiaoou Tang, and Chen Change Loy. Lite-flowNet: A lightweight convolutional neural network for optical flow estimation. In *Proceedings of the IEEE conference on computer vision and pattern recognition*, pages 8981–8989, 2018.
- [11] Tak-Wai Hui, Xiaoou Tang, and Chen Change Loy. A lightweight optical flow CNN-revisiting data fidelity and regularization. *arXiv preprint arXiv:1903.07414*, 2019.
- [12] Eddy Ilg, Nikolaus Mayer, Tonmoy Saikia, Margret Keuper, Alexey Dosovitskiy, and Thomas Brox. FlowNet 2.0: Evolution of optical flow estimation with deep networks. In *Proceedings of the IEEE conference on computer vision and pattern recognition*, pages 2462–2470, 2017.
- [13] J Yu Jason, Adam W Harley, and Konstantinos G Derpanis. Back to basics: Unsupervised learning of optical flow via brightness constancy and motion smoothness. In *European Conference on Computer Vision*, pages 3–10. Springer, 2016.
- [14] Rico Jonschkowski, Austin Stone, Jon Barron, Ariel Gordon, Kurt Konolige, and Anelia Angelova. What matters in unsupervised optical flow. *ECCV*, 2020.
- [15] Mans Larsson, Erik Stenborg, Lars Hammarstrand, Marc Pollefeys, Torsten Sattler, and Fredrik Kahl. A cross-season correspondence dataset for robust semantic segmentation. In *Proceedings of the IEEE/CVF Conference on Computer Vision and Pattern Recognition*, pages 9532–9542, 2019.
- [16] Hoang Le, Feng Liu, Shu Zhang, and Aseem Agarwala. Deep homography estimation for dynamic scenes. In *Proceedings of the IEEE/CVF Conference on Computer Vision and Pattern Recognition*, pages 7652–7661, 2020.
- [17] Zhengqi Li and Noah Snavely. Megadepth: Learning single-view depth prediction from internet photos. In *Proceedings of the IEEE Conference on Computer Vision and Pattern Recognition*, pages 2041–2050, 2018.
- [18] Tsung-Yi Lin, Michael Maire, Serge Belongie, James Hays, Pietro Perona, Deva Ramanan, Piotr Dollár, and C Lawrence Zitnick. Microsoft coco: Common objects in context. In *European conference on computer vision*, pages 740–755. Springer, 2014.
- [19] Ce Liu, Jenny Yuen, and Antonio Torralba. Sift flow: Dense correspondence across scenes and its applications. *IEEE transactions on pattern analysis and machine intelligence*, 33(5):978–994, 2010.
- [20] Pengpeng Liu, Irwin King, Michael R Lyu, and Jia Xu. DdfLOW: Learning optical flow with unlabeled data distillation. In *Proceedings of the AAAI Conference on Artificial Intelligence*, volume 33, pages 8770–8777, 2019.
- [21] Pengpeng Liu, Irwin King, Michael R Lyu, and Jia Xu. Flow2Stereo: Effective self-supervised learning of optical flow and stereo matching. In *Proceedings of the IEEE/CVF Conference on Computer Vision and Pattern Recognition*, pages 6648–6657, 2020.
- [22] David G Lowe. Distinctive image features from scale-invariant keypoints. *International journal of computer vision*, 60(2):91–110, 2004.
- [23] Jundan Luo, Zhaoyang Huang, Yijin Li, Xiaowei Zhou, Guofeng Zhang, and Hujun Bao. Niid-net: Adapting surface normal knowledge for intrinsic image decomposition in indoor scenes. *IEEE Transactions on Visualization and Computer Graphics*, 26(12):3434–3445, 2020.
- [24] Will Maddern, Geoffrey Pascoe, Chris Linegar, and Paul Newman. 1 year, 1000 km: The oxford robotcar dataset. *The International Journal of Robotics Research*, 36(1):3–15, 2017.
- [25] Simon Meister, Junhwa Hur, and Stefan Roth. Unflow: Unsupervised learning of optical flow with a bidirectional census loss. In *Proceedings of the AAAI Conference on Artificial Intelligence*, volume 32, 2018.
- [26] Iaroslav Melekhov, Aleksei Tiulpin, Torsten Sattler, Marc Pollefeys, Esa Rahtu, and Juho Kannala. Dgc-net: Dense geometric correspondence network. In *2019 IEEE Winter Conference on Applications of Computer Vision (WACV)*, pages 1034–1042. IEEE, 2019.

- [27] Iaroslav Melekhov, Juha Ylioinas, Juho Kannala, and Esa Rahtu. Relative camera pose estimation using convolutional neural networks. In *International Conference on Advanced Concepts for Intelligent Vision Systems*, pages 675–687. Springer, 2017.
- [28] Krystian Mikolajczyk and Cordelia Schmid. Scale & affine invariant interest point detectors. *International journal of computer vision*, 60(1):63–86, 2004.
- [29] Anastasya Mishchuk, Dmytro Mishkin, Filip Radenovic, and Jiri Matas. Working hard to know your neighbor’s margins: Local descriptor learning loss. In *NIPS*, 2017.
- [30] Hyeonwoo Noh, Andre Araujo, Jack Sim, Tobias Weyand, and Bohyung Han. Large-scale image retrieval with attentive deep local features. In *Proceedings of the IEEE international conference on computer vision*, pages 3456–3465, 2017.
- [31] Yuki Ono, Eduard Trulls, Pascal Fua, and Kwang Moo Yi. Lf-net: learning local features from images. In *Proceedings of the 32nd International Conference on Neural Information Processing Systems*, pages 6237–6247, 2018.
- [32] Tong Qin and Shaojie Shen. Online temporal calibration for monocular visual-inertial systems. In *2018 IEEE/RSJ International Conference on Intelligent Robots and Systems (IROS)*, pages 3662–3669. IEEE, 2018.
- [33] Rahul Raguram, Ondrej Chum, Marc Pollefeys, Jiri Matas, and Jan-Michael Frahm. Usac: a universal framework for random sample consensus. *IEEE transactions on pattern analysis and machine intelligence*, 35(8):2022–2038, 2012.
- [34] René Ranftl and Vladlen Koltun. Deep fundamental matrix estimation. In *Proceedings of the European conference on computer vision (ECCV)*, pages 284–299, 2018.
- [35] Anurag Ranjan and Michael J Black. Optical flow estimation using a spatial pyramid network. In *Proceedings of the IEEE conference on computer vision and pattern recognition*, pages 4161–4170, 2017.
- [36] Zhe Ren, Junchi Yan, Bingbing Ni, Bin Liu, Xiaokang Yang, and Hongyuan Zha. Unsupervised deep learning for optical flow estimation. In *Proceedings of the AAAI Conference on Artificial Intelligence*, volume 31, 2017.
- [37] Jerome Revaud, Cesar De Souza, Martin Humenberger, and Philippe Weinzaepfel. R2d2: Reliable and repeatable detector and descriptor. In H. Wallach, H. Larochelle, A. Beygelzimer, F. d’Alché-Buc, E. Fox, and R. Garnett, editors, *Advances in Neural Information Processing Systems*, volume 32. Curran Associates, Inc., 2019.
- [38] Ignacio Rocco, Relja Arandjelovic, and Josef Sivic. Convolutional neural network architecture for geometric matching. In *Proceedings of the IEEE conference on computer vision and pattern recognition*, pages 6148–6157, 2017.
- [39] Ignacio Rocco, Mircea Cimpoi, Relja Arandjelović, Akihiko Torii, Tomas Pajdla, and Josef Sivic. Neighbourhood consensus networks. In *Proceedings of the 32nd International Conference on Neural Information Processing Systems*, pages 1658–1669, 2018.
- [40] Paul-Edouard Sarlin, Cesar Cadena, Roland Siegwart, and Marcin Dymczyk. From coarse to fine: Robust hierarchical localization at large scale. In *Proceedings of the IEEE/CVF Conference on Computer Vision and Pattern Recognition*, pages 12716–12725, 2019.
- [41] Paul-Edouard Sarlin, Daniel DeTone, Tomasz Malisiewicz, and Andrew Rabinovich. Superglue: Learning feature matching with graph neural networks. In *Proceedings of the IEEE/CVF conference on computer vision and pattern recognition*, pages 4938–4947, 2020.
- [42] Torsten Sattler, Will Maddern, Carl Toft, Akihiko Torii, Lars Hammarstrand, Erik Stenborg, Daniel Safari, Masatoshi Okutomi, Marc Pollefeys, Josef Sivic, et al. Benchmarking 6dof outdoor visual localization in changing conditions. In *Proceedings of the IEEE Conference on Computer Vision and Pattern Recognition*, pages 8601–8610, 2018.
- [43] Johannes Lutz Schönberger and Jan-Michael Frahm. Structure-from-motion revisited. In *Conference on Computer Vision and Pattern Recognition (CVPR)*, 2016.
- [44] Xi Shen, François Darmon, Alexei A Efros, and Mathieu Aubry. Ransac-flow: generic two-stage image alignment. *arXiv preprint arXiv:2004.01526*, 2020.
- [45] Fridtjof Stein. Efficient computation of optical flow using the census transform. In *Joint Pattern Recognition Symposium*, pages 79–86. Springer, 2004.
- [46] Deqing Sun, Xiaodong Yang, Ming-Yu Liu, and Jan Kautz. Pwc-net: Cnns for optical flow using pyramid, warping, and cost volume. In *Proceedings of the IEEE conference on computer vision and pattern recognition*, pages 8934–8943, 2018.
- [47] Deqing Sun, Xiaodong Yang, Ming-Yu Liu, and Jan Kautz. Models matter, so does training: An empirical study of cnns for optical flow estimation. *IEEE transactions on pattern analysis and machine intelligence*, 42(6):1408–1423, 2019.
- [48] Zachary Teed and Jia Deng. Raft: Recurrent all-pairs field transforms for optical flow. In *European Conference on Computer Vision*, pages 402–419. Springer, 2020.
- [49] Prune Truong, Martin Danelljan, and Radu Timofte. Glunet: Global-local universal network for dense flow and correspondences. In *Proceedings of the IEEE/CVF conference on computer vision and pattern recognition*, pages 6258–6268, 2020.
- [50] Prune Truong, Martin Danelljan, Luc Van Gool, and Radu Timofte. Gocor: Bringing globally optimized correspondence volumes into your neural network. *Advances in Neural Information Processing Systems 33 pre-proceedings (NeurIPS 2020)*, 2020.
- [51] Benjamin Ummenhofer, Huizhong Zhou, Jonas Uhrig, Nikolaus Mayer, Eddy Ilg, Alexey Dosovitskiy, and Thomas Brox. Demon: Depth and motion network for learning monocular stereo. In *Proceedings of the IEEE Conference on Computer Vision and Pattern Recognition*, pages 5038–5047, 2017.
- [52] Levi Valgaerts, Andrés Bruhn, and Joachim Weickert. A variational model for the joint recovery of the fundamental matrix and the optical flow. In *Joint Pattern Recognition Symposium*, pages 314–324. Springer, 2008.
- [53] Qianqian Wang, Xiaowei Zhou, Bharath Hariharan, and Noah Snavely. Learning feature descriptors using camera pose supervision. In *European Conference on Computer Vision*, pages 757–774. Springer, 2020.
- [54] Andreas Wedel, Daniel Cremers, Thomas Pock, and Horst Bischof. Structure-and motion-adaptive regularization for

- high accuracy optic flow. In *2009 IEEE 12th International Conference on Computer Vision*, pages 1663–1668. IEEE, 2009.
- [55] Koichiro Yamaguchi, David McAllester, and Raquel Urtasun. Robust monocular epipolar flow estimation. In *Proceedings of the IEEE conference on computer vision and pattern recognition*, pages 1862–1869, 2013.
 - [56] Wending Yan, Aashish Sharma, and Robby T Tan. Optical flow in dense foggy scenes using semi-supervised learning. In *Proceedings of the IEEE/CVF Conference on Computer Vision and Pattern Recognition*, pages 13259–13268, 2020.
 - [57] Guandao Yang, Tomasz Malisiewicz, Serge J Belongie, Erez Farhan, Sungsoo Ha, Yuewei Lin, Xiaojing Huang, Hanfei Yan, and Wei Xu. Learning data-adaptive interest points through epipolar adaptation. In *CVPR Workshops*, pages 1–7, 2019.
 - [58] Zhichao Yin and Jianping Shi. Geonet: Unsupervised learning of dense depth, optical flow and camera pose. In *Proceedings of the IEEE conference on computer vision and pattern recognition*, pages 1983–1992, 2018.
 - [59] Jirong Zhang, Chuan Wang, Shuaicheng Liu, Lanpeng Jia, Nianjin Ye, Jue Wang, Ji Zhou, and Jian Sun. Content-aware unsupervised deep homography estimation. In *European Conference on Computer Vision*, pages 653–669. Springer, 2020.
 - [60] Yinqiang Zheng, Mingfang Zhang, and Feng Lu. Optical flow in the dark. In *Proceedings of the IEEE/CVF Conference on Computer Vision and Pattern Recognition*, pages 6749–6757, 2020.
 - [61] Yiran Zhong, Pan Ji, Jianyuan Wang, Yuchao Dai, and Hongdong Li. Unsupervised deep epipolar flow for stationary or dynamic scenes. In *Proceedings of the IEEE/CVF Conference on Computer Vision and Pattern Recognition*, pages 12095–12104, 2019.
 - [62] Yuliang Zou, Zelun Luo, and Jia-Bin Huang. Df-net: Unsupervised joint learning of depth and flow using cross-task consistency. In *Proceedings of the European conference on computer vision (ECCV)*, pages 36–53, 2018.